Available online at www.sciencedirect.com
SCIENCE DIRECT®
International Journal of Mass Spectrometry 241 (2005) 315–323
International Journal of Mass Spectrometry
www.elsevier.com/locate/ijms

Proton migration and its effect on the MS fragmentation of *N*-acetyl OMe proline: MS/MS experiments and ab initio and density functional calculations

István Komáromi[a], Árpád Somogyi[b], Vicki H. Wysocki[b,*]

[a] *Research Group for Thrombosis and Haemostasis of the Hungarian Academy of Sciences, University of Debrecen, Nagyerdei krt. 98, Debrecen, Hungary*
[b] *Department of Chemistry, University of Arizona, Tucson, AZ 85721, USA*
Received 18 December 2004; accepted 30 December 2004

Abstract

The comparison of low energy gas-phase collision-induced dissociation (eV CID) and low energy surface-induced dissociation (eV SID) of protonated *N*-acetyl *O*-methoxy (*N*-acetyl OMe) proline shows that this ion has two main fragmentation pathways. One of them is the loss of methanol that occurs at low internal energy. The other one is a higher energy process, the loss of ketene from the protonated molecule. Theoretical calculations at three different levels provide further support for the energy requirements of these fragmentation reactions. These calculations also suggest that several protonated forms may coexist together after the ion activation and several fragmentation pathways may be operative, especially for the ketene loss.

Keywords: MS/MS; Peptide fragmentation; Ab initio; Density function, *N*-acety OMe proline

1. Introduction

MS/MS fragmentation of singly and multiply protonated peptides has a great practical importance; based on the fragmentation pattern and sequence information in databases, the sequence of individual peptides can be determined, and protein identification can be rationalized by using different search algorithms, such as SEQUEST [1], Mascot [2], and MS-Tag [3]. An improved understanding of fragmentation rules for protonated peptides and their incorporation into these search programs may increase the reliability of protein identification by MS/MS.

Based on systematic studies by Biemann and Martin [4], Boyd and co-workers [5,6], Harrison and co-workers [7,8], Gaskell and co-workers [9,10], and Wysocki and co-workers [11–14], the so-called "mobile proton" model has emerged and now is widely accepted. In spite of its relative simplicity, this model provides a good qualitative description for peptide fragmentation. Briefly, this model states that upon ion activation, the proton(s) added to a peptide will migrate to various protonation sites prior to fragmentation and will trigger charge directed cleavages. If the proton is strongly sequestered by a basic amino side chain, or in the lack of the ionizing proton (fixed charged derivative peptides), other processes, such as charge remote fragmentation can also occur [14]. Simple molecular orbital calculations on different protonated forms [15,16] also played an important role in the emergence of the mobile proton model. These calculations clearly show that protonation on the amide nitrogen leads to a considerable weakening of the amide bond while protonation on the amide oxygen makes the amide bonds stronger than those in the neutral species. As a result, amide bond protonated forms are considered to be possible "fragmenting" structures even though they are less favored thermodynamically. The "mobile proton" model has been further

* Corresponding author. Tel.: +1 520 6212628; fax: +1 520 6218407.
E-mail address: vwysocki@u.arizona.edu (V.H. Wysocki).

1387-3806/$ – see front matter © 2005 Elsevier B.V. All rights reserved.
doi:10.1016/j.ijms.2004.12.033

validated by additional theoretical calculations by Paizs and co-workers [17–21]. Very recently, a kinetic model based on the mobile proton model has also been developed by Zhang to quantitatively simulate the low energy collision-induced dissociation spectra of protonated peptides [22].

As was pointed out by Paizs and Suhai in a recent review on peptide fragmentation [19], the mobile proton model addresses questions associated mainly with the predissociation step(s), i.e., the model focuses on the accessibility or inactivity of proton-transfer pathways, which lead to reactive intermediates of sequence ion fragmentation channels. To overcome this limitation, the use of the "pathways in competition" (PIC) model that involves a detailed energetic and kinetic characterization of the major fragmentation pathways (PFPs) is proposed. This approach maps the potential energy surface (PES) and thus provides more mechanistic and kinetic information on peptide fragmentation. It has been pointed out that several fragmentation pathways exist even for relatively simple systems (e.g., for RD–OH, see ref. [20]). Although a carefully built search engine has been proposed by Paizs and Suhai [21] to make these calculations automatic, this detailed computational approach still requires a lot of computational time. Therefore, other experimental and statistical approaches to study peptide fragmentation are justified.

The first statistical evaluations of the MS/MS data of large numbers of protonated peptides are just emerging [23–25]. The Wysocki group has been extensively involved in this work by evaluating many thousands of low energy collisional activation (eV CID) spectra. This group also has many years of experience in another ion activation technique, low energy surface-induced dissociation (eV SID) developed originally by Cooks and co-workers [26]. In fact, eV SID fragmentation of protonated peptides provided much experimental evidence of the "mobile proton" model [14].

In the present work, we present a combination of both experimental and theoretical results that are related to the investigation of the so-called "proline effect" [23,27–29]. To make the computational time reasonable, we chose the simplest model compound, *N*-acetyl *O*-methoxy (*N*-acetyl OMe) proline. The structure of this compound and its protonated form has been calculated by Siu and co-workers [30]. We applied three different levels of calculations as described in the computation details below. On the experimental side, we used different ion activation techniques available on different instruments. They include eV CID in a Thermoelectron ion trap instrument and in a Thermoelectron triple quadrupole (QQQ) instrument, sustained off-resonance irradiation (SORI), and resonance excitation (RE) in an IonSpec 4.7 T Fourier transform ion cyclotron resonance (FT-ICR) instrument, and eV SID on a modified Micromass Q-TOF instrument. As will be pointed below, a low energy process (methanol loss), and a high energy process (ketene loss) have been observed as main fragmentation pathways for protonated *N*-acetyl OMe proline. The ketene loss is preceded by a proton transfer so that the proton migration process was also investigated theoretically together with the description of the two main fragmentation pathways.

2. Experimental

Methyl prolinate hydrochloride was purchased from Aldrich and was acetylated without further purification by using 5% sodium bicarbonate and acetyl chloride.

MS/MS fragmentation spectra of the protonated $[M+H]^+$ *N*-acetyl OMe proline (*m*/*z* 172) were obtained on four different instruments with different ion activation techniques. In all cases, electrospray ionization (ESI) was used to generate the $[M+H]^+$ precursor ions. Sample solutions, with a concentration range of 40–60 μM in MeOH:H_2O 1:1 containing 2% of acetic acid, were infused with a flow rate of 2–5 μl/min.

A Thermoelectron (Finnigan) LCQ Classic ion trap instrument was used to obtain low energy/multiple collision spectra. Helium was used as collision gas and 10–30% of the maximum excitation amplitude was applied. An IonSpec 4.7 T FT-ICR instrument was used to obtain SORI and RE MS/MS spectra. Nitrogen gas was used as collision gas and a 1000 Hz frequency shift was used in the SORI experiments. A short excitation pulse (20–30 μs) was used in the RE experiments. A Finnigan TSQ 7000 QQQ instrument was also used to obtain gas-phase collisional activation spectra with Ar. In this case, the laboratory collision energy was varied in the range of 10–30 eV. For surface-induced dissociation (SID) experiments, a custom-modified Micromass Q-TOF instrument was used. A self-assembled monolayer prepared by reaction of 2-(perfluorooctyl) ethane thiol with a gold surface was used as the collision target.

3. Computational details

Throughout the paper, the following notations are used: for global and local minima of protonated *N*-acetyl OMe structures, MH_*I* is used, where *I* = 0–*n*, MH_0 indicating the most stable structure reported by Siu and co-workers [30] (global minimum), MH_1 is the second most stable structure, MH_2 is the third most stable structure, etc. Note that all relative energies are referenced to the MH_0 global mimimum (Table 1). TS_*I*_*J* indicates a transition state which connects the *I*th and *J*th minima, while TS_*I*_K and TS_*I*_M indicate transition states correspond to a ketene (K) or methanol (M) loss from the *I*th minimum, respectively. Despite the relative simplicity of the investigated ion and the fragmentation processes, many local minima and many transition states can be found on the potential energy surface. In this paper, the only structures taken into account were those based on energetic considerations, which might play important roles on the investigated processes.

Three processes have been studied: (i) the proton transfer from the global minimum (MH_0) to one of the local minima MH_(1–4) that corresponds to the ring N protonated form),

Table 1
Energy and ZPVE corrected energy values (in kJ/mol) for a few stationary points on the potential energy surface of the protonated proline derivative calculated by B3LYP, HF, and MP2 levels of theories using the same 6-31++G(d,p) basis set

Structure	B3LYP		HF		MP2	
	E	*E* + ZPVE	*E*	*E* + ZPVE	*E*	*E* + ZPVE
MH_0	0.00	0.00	0.00	0.00	0.00	0.00
MH_1	19.24	19.40	15.55	15.39	12.35	11.71
MH_2	57.25	56.77	54.36	54.04	39.93	38.16
MH_3	71.04	70.72	70.24	69.91	51.79	50.03
MH_4	84.03	84.19	78.89	79.38	58.05	57.41
MH_5	89.16	88.36	87.39	86.91	63.18	61.26
TS_0_1	40.25	39.61	32.07	30.31	30.31	28.54
TS_0_2	93.49	82.10	116.42	102.95	82.26	69.91
TS_0_4	245.50	230.11	282.87	266.83	232.84	216.96
TS_1_M	143.20	136.94	185.05	170.78	129.09	121.55
TS_2_K	180.56	172.54	205.74	182.00	171.74	151.38
TS_3_K	177.03	169.01	205.74	182.00	171.74	151.38
TS_4_K	171.42	154.42	200.76	177.99	163.72	142.56
TS_5_K	170.62	155.06	200.92	178.15	161.16	140.31

See Figs. 2 and 3 and the text for structure notation. The energy values for the global minima are −589.9927186, −593.5390676, and −591.8113034 a.u. at the HF, B3LYP, and MP2 levels, respectively.

(ii) the loss of methanol through the TS_0_M transition state, and (iii) the loss of ketene through the TS_(1–4)_K transition states.

For the global minimum, the structure reported by Siu and co-workers has been confirmed [30]. Note we have found that all the other geometries corresponding to other stationary points on the potential energy surface have higher energy than this global minimum structure.

For MH_0 → MH_2, the methanol loss and the ketene loss pathway potential surface scans have been performed using two of the internal coordinates thought to be important in the given reaction path. The potential energy surface scan calculations have been carried out either using ONIOM (B3LYP/6-31++G(d,p):B3LYP/6-31G(d)) [31] or pure B3LYP/6-31++G(d,p) calculations. The stationary points were optimized at HF/6-31++G(d,p), B3LYP/6-31++G(d,p), and MP2/6-31++G(d,p) levels of theories. Vibrational analysis has been performed at the same levels and all stationary points have either zero (local or global energy minima) or only one (transition states) imaginary vibrational frequency (negative eigenvalues of the corresponding hessians). The numbering scheme applied is shown in Scheme 1.

All the calculations have been carried out using Gaussian'98 and the Gaussian'03 packages [32,33]. For visualization, the Molekel program sets were used [34,35].

4. Results and discussion

Fig. 1 shows the MS/MS spectra of the protonated *N*-acetyl *O*-methoxy proline obtained by different ion activation methods: gas-phase collisional activation on (a) a Finnigan LCQ Ion Trap instrument, (b) a Finnigan triple quadrupole (13 eV laboratory collision energy), and (c) surface-induced dissociation on a Micromass Q-SID-TOF instrument (13 eV). Low energy gas-phase collisional activation in the ion trap instrument leads to the loss of MeOH (*m*/*z* 140) and a subsequent loss of CO (*m*/*z* 112) (Fig. 1a). Note that SORI in the IonSpec 4.7 T FT-ICR resulted in a spectrum very similar to that detected in the ion trap. Resonance excitation in the FT-ICR cell resulted in the same fragment ions but a weak peak at *m*/*z* 130 also appeared in the MS/MS spectrum (not shown). This fragment ion is more prominent in the MS/MS spectrum obtained on the triple quadrupole instrument (Fig. 1b). This ion corresponds to the loss of ketene (CH_2=C=O) from the protonated molecule. An additional fragment ion at *m*/*z* 70 also appears in the QQQ MS/MS spectrum. This peak corresponds to the proline immonium ion, P. The SID spectrum (Fig. 1c) shows great similarities with the QQQ MS/MS spectrum. The ketene loss is apparent, but the internal fragment, P,

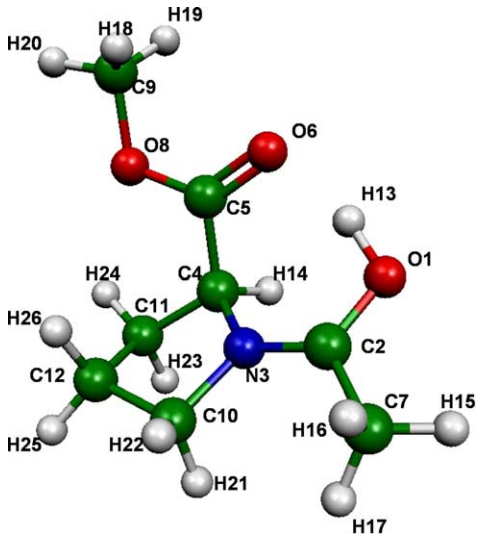

Scheme 1.

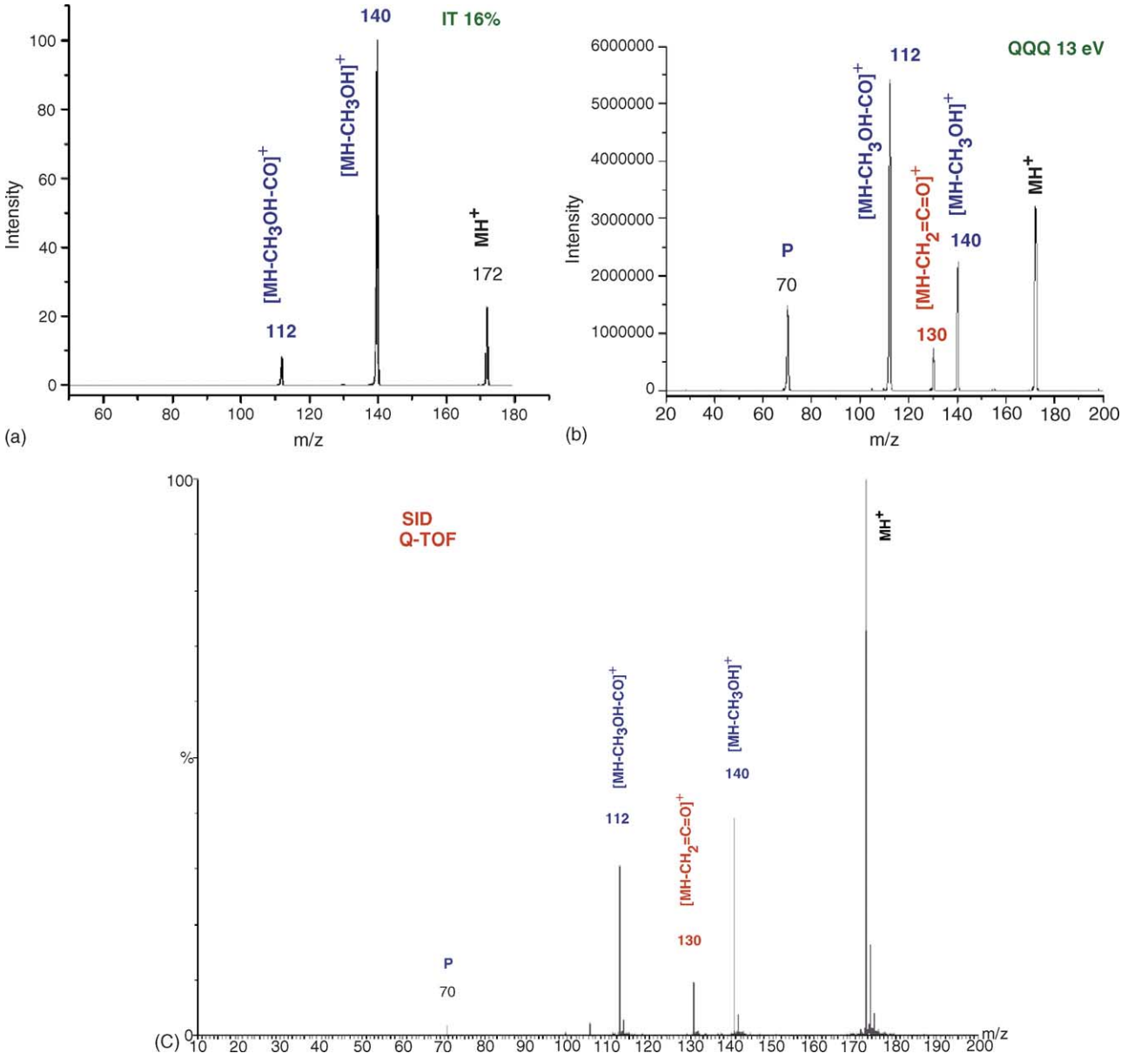

Fig. 1. MS/MS spectra of *N*-acetyl OMe proline obtained by different ion activation methods such as gas-phase collisional activation on (a) a Finnigan LCQ Ion Trap instrument, (b) a Finnigan QQQ (13 eV laboratory collision energy), and (c) surface-induced dissociation on a Micromass Q-SID-TOF instrument (13 eV).

is less intense in the SID spectrum than in the QQQ spectrum, probably because of the multiple collision conditions used in the QQQ.

The MS/MS results clearly show that there are two main primary fragmentation channels: (i) a low energy fragmentation pathway associated with methanol loss and (ii) a high energy pathway related to ketene loss. Both fragmentation pathways must be associated with rearrangements that can be triggered by proton migration in the protonated molecule because neither can be explained by a direct cleavage of any of the low energy forms of the protonated molecule. To investigate the energetics of these rearrangement/proton migration processes, we performed detailed quantum chemical calculations. Several stationary points (global and local minima and saddle points) have been found on the potential energy surface. These, together with the corresponding structures, will be discussed below in detail.

4.1. Structures corresponding to energy minima

The structures corresponding to the global and local energy minima, together with some selected transition states, are shown in Figs. 2 and 3. The relative energies of selected stationary points calculated by three different methods are collected in Table 1. Table 1 also contains the absolute energies calculated for the global minimum.

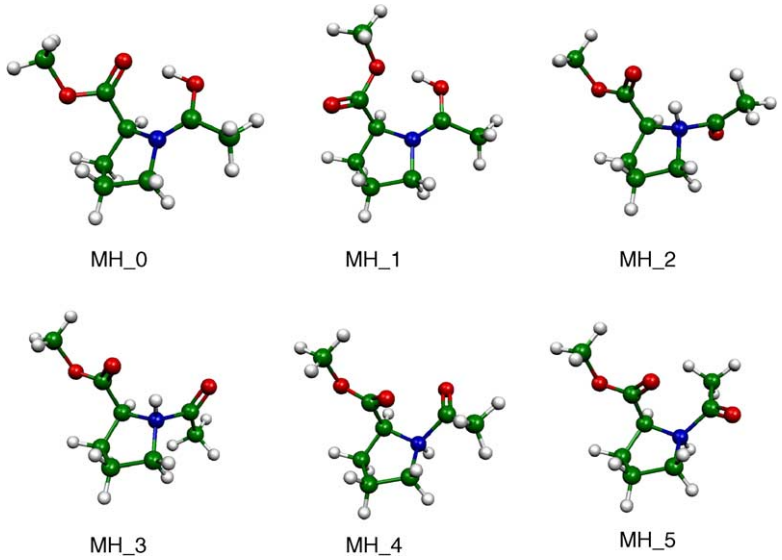

Fig. 2. MP26-31++G(d,p) structures of the protonated *N*-acetyl OMe proline corresponding to the global minimum (MH_0) and selected local minima (MH_(1–5)).

MH_0 corresponds to the global minimum and was found to be essentially the same as reported by Siu and co-workers [30]. In this most stable structure, the acetyl group is protonated and the ionizing proton is involved in a hydrogen bond between the acetyl O1 and ester carbonyl O6 atoms (the numbering of atoms is shown in Scheme 1). A conformational isomer can be easily derived from the global minimum, in which the H13 ionizing proton participates in a hydrogen bond between the acetyl O1 and the ester O8 atoms (MH_1). This conformation also represents a minimum on the potential energy surface of the protonated molecule $[M+H]^+$ and has higher (ZPVE corrected) energy by 11.71–19.40 kJ/mol than the global minimum (depending on the computational method applied; Table 1). This relatively small energy gap between these structures indicates that the MH_1 conformation can be populated even at relatively low internal energy. In other words, this means that even at low energy ion activation, the MH_1 conformer may coexist with the most stable protonated form MH_0.

Other structures in which the proton is located on the ring nitrogen (N3) are also of particular interest because they may be intermediates in the ketene loss pathway. Geometry optimization starting from three different geometries for both possible protonation sites of the N3 ring nitrogen leads to two new local minima for each structural isomer. Therefore, altogether at least four different low energy protonated structures should be considered (MH_(2–5)). These structures are depicted in Fig. 2 and their relative energies are compared to the global minimum in Table 1. The structures MH_(2–5) have substantially higher relative energies than the MH_1 local minimum. In each isomer, the main differences between these local minima correspond to different acetyl conformations (Fig. 2).

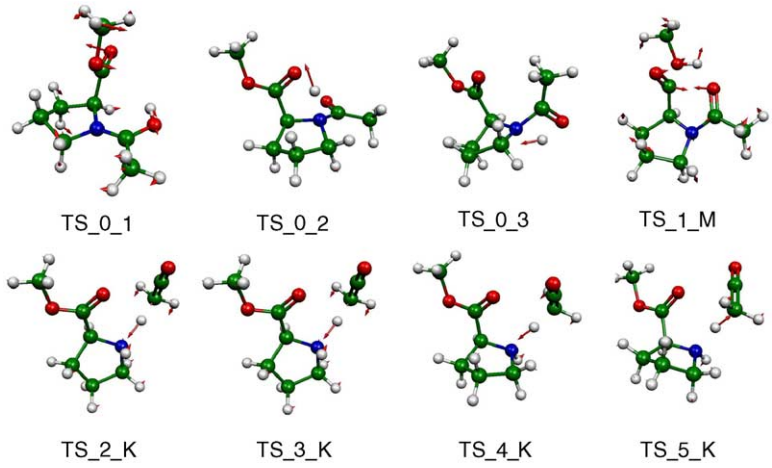

Fig. 3. MP26-31++G(d,p) structures of selected transitions states (see text for details).

It should be mentioned that no local energy minimum was found in which the ionizing proton is involved in a hydrogen bond between the acetyl oxygen (O1) and the ring nitrogen (N3). Starting from such a structure, geometry optimization resulted in a conformer that corresponds to the global energy minimum, MH_0.

4.2. Transition states between the global energy minimum (MH_0) and the local energy minima MH_1, MH_2, and MH_4

4.2.1. MH_0 → MH_1 conversion, TS_0_1

This is an important structural conversion in which the proton bridged between the two carbonyl oxygen atoms (O1 and O6) in MH_0 becomes bridged between the acetyl carbonyl (O1) and the ester oxygen (O8) in MH_1 and triggers methanol loss. This conversion corresponds to a rotation around the C4–C5 bond as shown by the vibrational displacement vectors in Fig. 3. The calculated activation energy is about 40 kJ/mol (B3LYP; Table 1). This relatively small value suggests that the rate of the interconversion between MH_0 and MH_1 is high at low ion activation energy.

4.2.2. MH_0 → MH_2 conversion, TS_0_2

In contrast to the previous case when only a rotation around the C4–C5 bond occurs, this transformation corresponds to a proton transfer from the acetyl O1 to the ring nitrogen, N3. Fig. 4 shows the potential energy surface scan related to this proton migration. The minimum energy path corresponds to the movement of the proton, first towards the nearby carbonyl oxygen (O6) and from there to the ring nitrogen (N3). Note that this proton migration does not necessarily require the existence of an O6 protonated local energy minimum. It is immediately apparent from Fig. 4 and Table 1 that this transition requires more than twice the activation energy than the MH_0 → MH_1 rotation (see, e.g., MP2 values of 69.91 kJ/mol versus 28.54 kJ/mol; Table 1).

4.2.3. MH_0 → MH_4 conversion, TS_0_4

The vibrational displacement vectors corresponding to the imaginary frequency of this isomerization indicate proton transfer from the protonated acetyl oxygen (O1) to the ring nitrogen (N3) (Fig. 2). In this case, the proton transfer occurs through a four-member ring. This is less favorable than the MH_0 → MH_2 transition state that corresponds to a seven-member ring. The data in Table 1 indicate that, independent of computation method, this stationary point has the highest relative energy, more than 216 kJ/mol. Hence, this proton migration process is less favorable than the decomposition of the protonated molecule (see discussion below).

4.3. Methanol loss

It was mentioned above that there is only a small energy gap between the global energy minimum structure (MH_0) and its rotamer around the C4–C5 axis (MH_1). Hence, under low energy activation conditions, MH_0 and MH_1 interconvert. The transition state corresponding to the methanol loss (TS_1_M; Fig. 5) is the lowest energy transition state (ca. 120–170 kJ/mol; Table 1) among those that lead to fragmentation products. The vibrational displacement vectors in the transition state indicate that while methanol leaves a lactone ring formation occurs in a concerted reaction. Note again that methanol loss is triggered by a "rotational" proton transfer from the acetyl oxygen (O1) to the ester O8 oxygen.

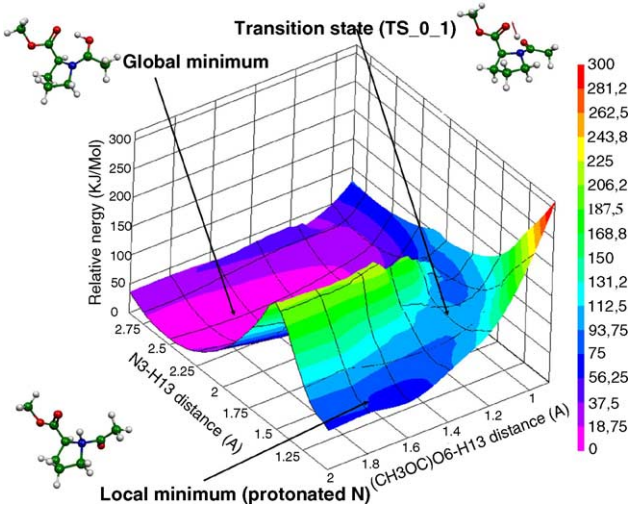

Fig. 4. Potential energy surface calculated by the ONIOM (B3LYP/6-31++G(d,p):B3LYP/6-31G(d)) method for the proton transition from the global minimum (MH_0) to the most stable ring nitrogen protonated from (MH_2).

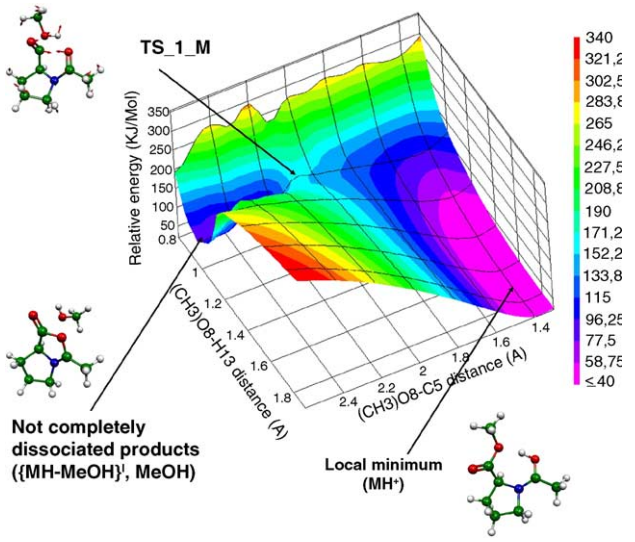

Fig. 5. Potential energy surface calculated by the ONIOM (B3LYP/6-31++G(d,p):B3LYP/6-31G(d)) method for the methanol loss from the local minimum MH_1.

4.4. Ketene loss

It is reasonable that the ring nitrogen (N3) protonated forms play an essential role in ketene loss. In the ring nitrogen (N3) protonated forms, the amide bond is significantly weakened [16,17] which helps in the elimination of the acetyl group. The departure of the acetyl group leaves behind a "satisfied" nitrogen bound to three atoms, with a lone pair available to remove a proton from acetyl producing a neutral ketene and a positively charged counterpart. In order to find appropriate transition states for ketene loss from the ring nitrogen protonated forms, potential energy surfaces have been generated by changing simultaneously the N3–H and the N3–C2 distances. It is important to note that this N(3)–H bond is the second N–H bond, i.e., the hydrogen atom involved in this bond is one of the H15, H16, and H17 acetyl methyl hydrogen atoms. For simplicity and computational considerations, only the parts of the potential energy surfaces thought to be important have been drawn. It is reasonable to assume that the N3–C2 bond should be weakened (i.e., the corresponding bond length should be increased) before the new N3–H bond is formed. Therefore, the potential energy surface calculations were started from an N3–C2 bond distance of 2.4 A.

The four local energy minima geometries MH_(2–5) suitable for ketene loss are not shown in Fig. 6; the figure shows only the four different potential energy surfaces calculated for ketene loss. The MH_(2–5) local minima are in the direction of the upper corner of each figure (i.e., at relatively long N3–H (H15, H16, or H17) and sufficiently short (1.5–1.6A) N3–C2 distances). It is apparent from Fig. 6 that the acetyl group is separated significantly from the rest of the molecule before of one of the acetyl methyl hydrogens moves to the N3 atom. In this part of the potential energy surface, however, the landscape is quite flat and might contain several local energy minima connected by very low energy transition states. Among those transition states, there must be some in which the imaginary frequency is dominated by the N3···H···CH_2(CO) vibration. These transition states are shown in Fig. 3 (TS_(2–5)_K). Notice that ketene is only loosely connected to the rest of the molecule in these transition states. In other words, these transition states can also be described as loosely bound ion-molecule complexes. The other consequence of this flat surface is the very similar energy values obtained starting from quite different local minima. We note, for example, that the TS_2_K and TS_3_K transition states are exactly the same at the HF and MP2 levels of theory (see Table 1; Fig. 3).

Finally, we note that the ZPVE corrected energy values corresponding to the transition states associated with ketene loss are higher than the transition state energies corresponding to the methanol loss at all three levels of theory. For example, at the MP2 level, the ZPVE corrected transition state energies for the ketene loss are in the range of 140–152 kJ/mol compared to those for the methanol loss of ca. 121 kJ/mol (Table 1). This result is consistent with the experimental

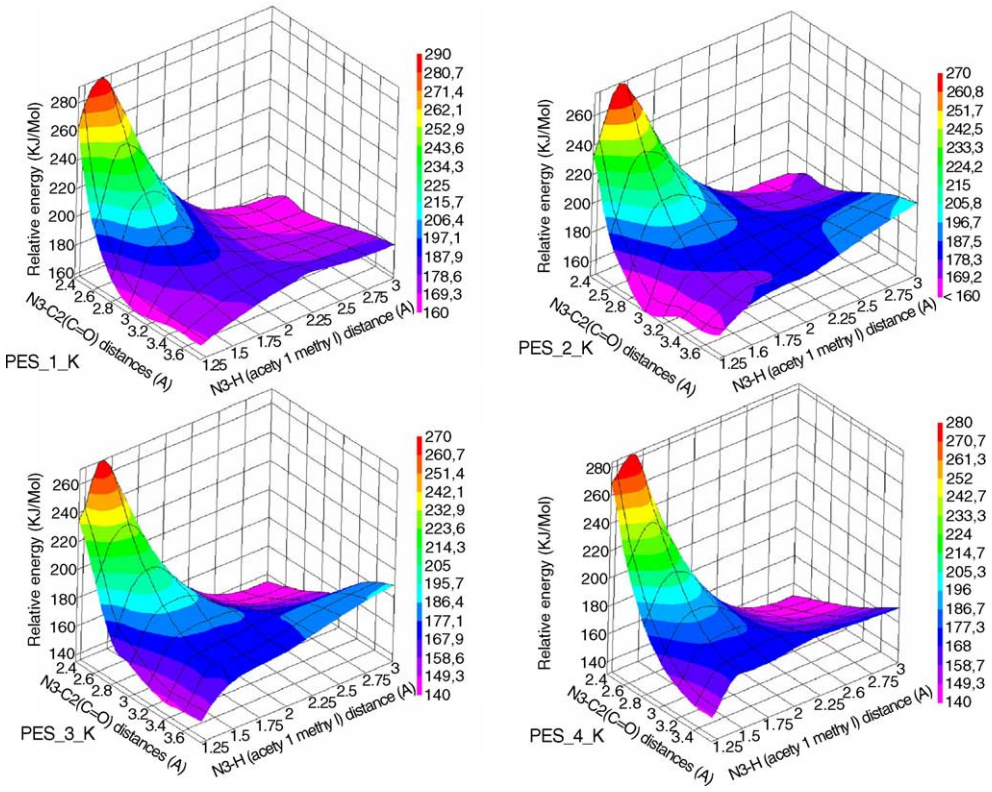

Fig. 6. Potential energy surfaces calculated by the B3LYP 6-31++G(d,p) method for four different pathways of ketene loss.

MS/MS results: a low energy loss of methanol and a higher energy loss of ketene from the protonated *N*-acetyl OMe proline. The computational results also suggest that a mixture of MH_0 and MH_1 protonated forms exists in the activated molecules and that multi-step, low energy collisions in the longer time-frame ion trap and FT-ICR instruments result mostly in the MeOH loss. On the other hand, higher internal energy deposition in one or a few steps in the QQQ and Q-TOF SID instruments allows the higher energy ketene loss to compete with methanol loss.

5. Conclusions

The experimental MS/MS and theoretical results presented in this work provide insight into the complexity of the fragmentation of protonated peptides. Even though *N*-acetyl OMe proline is a relatively simple amino acid derivative that has two main fragmentation channels (the low energy methanol loss and the higher energy ketene loss), several local minima and transition states have been found by theoretical calculations. Proton rearrangements can occur with relatively low energy barriers so heterogeneous population of different protonated forms may coexist before ion fragmentation. This system, therefore, provides an additional example for the validation of the "mobile proton" model. Groups such as the ester carbonyl can assist a cleavage by enabling proton transfer to a site of lower basicity (such as the amide N).

Acknowledgements

This work was part of collaborative research sponsored by the National Science Foundation (NSF) and the Hungarian Academy of Sciences (NSF-MTA OTKA, INT-0122172). Research in the Wysocki lab was supported by NSF grant DBI-0244437. The authors thank Quingfen Zhang and Asiri Galhena of the Wysocki lab for recording the QQQ and SID spectra, respectively, and Ronald Wysocki for synthesis.

References

[1] J.K. Eng., A.L. McCormack, J.R. Yates III, J. Am. Soc. Mass Spectrom. 5 (1994) 976.
[2] D.N. Perkins, D.J. Pappin, D.M. Creasy, J.S. Cottrell, Electrophoresis 20 (1999) 3551.
[3] K.R. Cleauser, P.R. Baker, A.L. Burlingame, Anal. Chem. 71 (1999) 2871.
[4] K. Biemann, S.A. Martin, Mass Spectrom. Rev. 6 (1987) 1.
[5] X. Tang, P. Thibault, R.K. Boyd, Anal. Chem. 65 (1993) 2824.
[6] X. Tang, R.K. Boyd, Rapid Commun. Mass Spectrom. 6 (1992) 651.
[7] C.W. Tsang, A.G. Harrison, J. Am. Chem. Soc. 98 (1976) 1301.
[8] A.G. Harrison, T. Yalcin, Int. J. Mass Spectrom. Ion Processes 165 (1997) 339.
[9] O. Burlet, C.Y. Yang, S.J. Gaskell, J. Am. Soc. Mass Spectrom. 3 (1992) 337.
[10] K.A. Cox, S.J. Gaskell, M. Morris, A. Whiting, J. Am. Soc. Mass Spectrom. 7 (1996) 522.
[11] J.L. Jones, A.R. Dongré, Á. Somogyi, V.H. Wysocki, J. Am. Chem. Soc. 116 (1994) 8368.
[12] A.R. Dongré, Á. Somogyi, V.H. Wysocki, J. Mass Spectrom. 31 (1996) 339.
[13] G. Tsaprailis, H. Nair, Á. Somogyi, V.H. Wysocki, W. Zhong, J.H. Futrell, S.G. Summerfield, S.J. Gaskell, J. Am. Chem. Soc. 121 (1999) 5142.
[14] V.H. Wysocki, G. Tsaprailis, L.L. Smith, L.A. Breci, J. Mass Spectrom. 35 (2000) 1399.
[15] A.L. McCormack, Á. Somogyi, A.R. Dongre, V.H. Wysocki, Anal. Chem. 65 (1993) 2859.
[16] Á. Somogyi, V.H. Wysocki, I. Mayer, J. Am. Soc. Mass Spectrom. 5 (1994) 704.
[17] I.P. Csonka, B. Paizs, G. Lendvay, S. Suhai, Rapid Commun. Mass Spectrom. 14 (2000) 417.
[18] B. Paizs, S. Suhai, Rapid Commun. Mass Spectrom. 15 (2001) 651.
[19] Paizs, B., Suhai, S. Mass Spectrom. Rev., in press (available online).
[20] B. Paizs, S. Suhai, B. Hargittai, V.J. Hruby, Á. Somogyi, Int. J. Mass Spectrom. 219 (2002) 203.
[21] B. Paizs, S. Suhai, Rapid Commun. Mass Spectrom. 16 (2002) 375.
[22] Z. Zhang, Anal. Chem. 76 (2004) 3908.
[23] Y. Huang, J.M. Triscari, L. Pasa-Tolic, G.A. Anderson, M.S. Lipton, R.D. Smith, V.H. Wysocki, J. Am. Chem. Soc. 126 (2004) 3034.
[24] D.L. Tabb, L.L. Smith, L.A. Breci, V.H. Wysocki, D. Lin, J.R. Yates, Anal. Chem. 75 (2003) 1155.
[25] E.A. Kapp, F. Schutz, G.E. Reid, J.S. Eddes, R.L. Moritz, R.A.J. O'Hair, T.P. Speed, R.J. Simpson, Anal. Chem. 75 (2003) 6251.
[26] M.A. Mabud, M.J. Dekrey, R.G. Cooks, Int. J. Mass Spectrom. Ion Processes 67 (1985) 285.
[27] L.A. Breci, D.L. Tabb, J.R. Yates, V.H. Wysocki, Anal. Chem. 75 (2003) 1963.
[28] T. Vaisar, J. Urban, J. Mass Spectrom. 31 (1996) 1185.
[29] H. Nair, A. Somogyi, V.H. Wysocki, J. Mass Spectrom. 31 (1996) 1141.
[30] V. Addario, Y.Z. Guo, I.K. Chu, Y. Ling, G. Ruggerio, C.F. Rodriquez, A.C. Hopkinson, K.W.M. Siu, Int. J. Mass Spectrom. 219 (2002) 101.
[31] S. Dapprich, I. Komáromi, S.K. Byun, K. Morokuma, M.J. Frisch, J. Mol. Struct. (Theochem) 462 (1999) 1.
[32] M.J. Frisch, G.W. Trucks, H.B. Schlegel, G.E. Scuseria, M.A. Robb, J.R. Cheeseman, V.G. Zakrzewski, J.A. Montgomery, R.E. Stratmann, J.C. Burant, S. Dapprich, J.M. Millam, A.D. Daniels, K.N. Kudin, M.C. Strain, O. Farkas, J. Tomasi, V. Barone, M. Cossi, R. Cammi, B. Mennucci, C. Pomelli, C. Adamo, S. Clifford, J. Ochterski, G.A. Petersson, P.Y. Ayala, Q. Cui, K. Morokuma, D.K. Malick, A.D. Rabuck, K. Raghavachari, J.B. Foresman, J. Cioslowski, J.V. Ortiz, B.B. Stefanov, G. Liu, A. Liashenko, P. Piskorz, I. Komaromi, R. Gomperts, R.L. Martin, D.J. Fox, T. Keith, M.A. Al-Laham, C.Y. Peng, A. Nanayakkara, C. Gonzalez, M. Challacombe, P.M.W. Gill, B.G. Johnson, W. Chen, M.W. Wong, J.L. Andres, M. Head-Gordon, E.S. Replogle, J.A. Pople, Gaussian 98 (Revision A.8), Gaussian Inc., Pittsburgh PA, 1998.
[33] M.J. Frisch, G.W. Trucks, H.B. Schlegel, G.E. Scuseria, M.A. Robb, J.R. Cheeseman, J.A. Montgomery, Jr., T. Vreven, K.N. Kudin, J.C. Burant, J.M. Millam, S.S. Iyengar, J. Tomasi, V. Barone, B. Mennucci, M. Cossi, G. Scalmani, N. Rega, G.A. Petersson, H. Nakatsuji, M. Hada, M. Ehara, K. Toyota, R. Fukuda, J. Hasegawa, M. Ishida, T. Nakajima, Y. Honda, O. Kitao, H. Nakai, M. Klene, X. Li, J.E. Knox, H.P. Hratchian, J.B. Cross, V. Bakken, C. Adamo, J. Jaramillo, R. Gomperts, R.E. Stratmann, O. Yazyev, A.J. Austin, R. Cammi, C. Pomelli, J.W. Ochterski, P.Y. Ayala, K. Morokuma, G.A. Voth, P. Salvador, J.J. Dannenberg, V.G. Zakrzewski, S. Dapprich, A.D. Daniels, M.C. Strain, O. Farkas, D.K. Malick, A.D. Rabuck, K. Raghavachari, J.B. Foresman, J.V. Ortiz, Q. Cui, A.G. Baboul, S. Clifford, J. Cioslowski, B.B. Stefanov, G. Liu, A. Liashenko, P.

Piskorz, I. Komaromi, R.L. Martin, D.J. Fox, T. Keith, M.A. Al-Laham, C.Y. Peng, A. Nanayakkara, M. Challacombe, P.M.W. Gill, B. Johnson, W. Chen, M.W. Wong, C. Gonzalez, and J.A. Pople, Gaussian 03 (Revision C.02), Gaussian Inc., Wallingford CT, 2004.
[34] Peter F. Flükiger, Development of the molecular graphics package MOLEKEL and its application to selected problems in organic and organometallic chemistry, Thèse No. 2561, Département de chimie physique, Université de Genève, Genève, 1992.
[35] S. Portmann, H.P. Lüthi, MOLEKEL: An Interactive Molecular Graphics Tool, CHIMIA 54 (2000) 766.